The International Journal of Advanced Manufacturing Technology (2019) 100:287–296
https://doi.org/10.1007/s00170-018-2664-8

ORIGINAL ARTICLE

# Investigating the effect of fabrication temperature on mechanical properties of fused deposition modeling parts using X-ray computed tomography

**Amir Reza Zekavat**[1] · **Anton Jansson**[1] · **Joakim Larsson**[1] · **Lars Pejryd**[1]

Received: 16 May 2018 / Accepted: 4 September 2018 / Published online: 24 September 2018


**Abstract**

Fused deposition modeling (FDM) is one of the most common additive manufacturing (AM) techniques for fabricating prototypes as well as functional parts. In this technique, several parameters may influence the part quality and consequently mechanical properties of fabricated components. In this paper, an experimental investigation on effects of fabrication temperature as one of the influential parameters on mechanical properties of manufactured parts is presented. A series of specimens fabricated at temperatures ranging from 180 to 260 °C were used for this investigation. X-ray computed tomography (CT) was used in order to non-destructively analyze the internal geometry of the specimens especially the bond between extruded filaments. Finally, the specimens were subjected to a uniaxial tensile load for evaluation of mechanical properties. The results showed that the specimens fabricated at lower temperatures have relatively lower tensile strength despite their considerably higher strain at break. In addition, the specimens fabricated at higher temperature range had significantly higher tensile strength because of the better bond between extruded filaments. The different mechanical responses were highly related to the internal geometry of the specimens and not necessarily the porosity. CT showed great potential as a non-destructive tool for investigation and development of FDM process.

**Keywords** Fused deposition modeling · Computed tomography · Polylactic acid · Additive manufacturing

## 1 Introduction

Additive manufacturing (AM) technologies have become competitive techniques for manufacturing of near net-shape parts. There has been a rapid growth in application of these methods due to their ability to fabricate parts with high geometrical complexity [1]. In these methods, a part is fabricated directly from computer-aided design (CAD) data in layer by layer fashion by adding material to the previous layer until the complete object is achieved. Although many of these techniques were initially developed and used for prototyping nowadays AM methods are also widely used for the production application. The rapid development of AM requires in-depth investigation at various aspects of these methods [2, 3]. Fused deposition modeling (FDM), has been used in various fields of science and engineering in the last decade [4, 5]. In FDM, the material is pushed to a heated liquefier and semi-molten material is extruded using a nozzle and deposited according to a path obtained from the slicing of the CAD geometry. Either the nozzle or build plate is moved in a transitional and transverse direction in order to selectively deposit the semi-molten material. A new layer of material is deposited on the previously deposited layers. The common materials which are used in this method are acrylonitrile butadiene styrene (ABS) and polylactic acid (PLA). Low cost of both raw material and the machines, as well as simplicity of the method, has made it a widespread method. Acceptable part accuracy, low maintenance cost, and ease of operating are other advantages of this method. The aforementioned advantages have given freedom to users worldwide to study different aspects of this method such as part accuracy and mechanical properties and its relation to the build direction.

✉ Amir Reza Zekavat
amirreza.zekavat@oru.se

[1] Örebro universitet Akademin för Naturvetenskap och Teknik, Fakultetsgatan 1, 701 82 Örebro, Sweden

Investigations have been done concerning the effects of process parameters on part quality and improvement of FDM process [5–10]. Bellehumeur et al. studied manufacturing parameters such as extrusion temperature and effect of extruded filament dimensions on the bond formation of polymer extruded filaments in FDM [11]. The main focus of that study was to model the bond formation process and it was concluded that nozzle temperature has a significant effect on bonding process. Both Mohamed et al. and Miquel et al. have confirmed the effect of build direction and part orientation in build chamber on the mechanical properties of parts made by FDM [8, 12]. Kaveh et al. suggested a method in order to improve internal cavity and precision of parts by optimizing printing parameters such as feed and flow rate, extruded filament width, and printing temperature [9]. Mechanical anisotropy of FDM parts and the effect of porosity ratio were studied by Koch et al. [13]. Ang et al. also showed that the mechanical properties of FDM-manufactured parts are influenced by porosity and build orientation [14]. They concluded that air gaps or basically porosity has the most influential effect on mechanical properties of FDM parts. IR thermography investigation on nozzle temperature and temperature of extruded filaments in order to study the bond formation in FDM process was done by Seppala et al. [15]. Effect of solidity ratio using an open-source slicing program has also been studied [7, 13].

Printing defects associated with FDM process especially internal defects related to turns at the points where contour and raster filaments intersect with each other have been discussed in the literature [16]. Koch et al. has shown that such effect has a strong influence on the strength of parts fabricated with extruded filaments perpendicular to load direction [13]. This effect which is also known as corner effect is the result of decelerating and accelerating of the nozzle at turns, which leads to a more material deposition at those points.

Although others have used weight, porosity, or solidity ratio in order to study the strength of FDM parts, an in-depth investigation of internal structure and bond quality of extruded filaments has not been carried out. X-ray computed tomography (CT) is a non-destructive inspection method for investigating internal features of objects. The technique was initially used in medical science but in the last decade, it has been widely used in engineering and many other branches of science [17]. The method is based on the ability of X-ray radiation to penetrate through objects and its attenuation based on the material and thickness of the object. Using this non-destructive method, it is possible to obtain geometrical information of both internal and external features of an object. CT was combined with finite element (FE) computation in a research work done by Nouri et al. [18]. A special modeling technique was used in order to quantify microstructural imperfections in FDM parts fabricated with different printing orientations.

In this study, the effect of fabrication temperature as an influential parameter in FDM on parts' mechanical properties has been investigated. CT has been used in order to non-destructively investigate the internal geometry of parts especially the bond between extruded filaments. The information from the internal geometry of the specimens obtained from CT scanning was used to find the relation between the selected fabrication temperatures and the resulting mechanical strength of the specimens obtained from mechanical testing. This study provides an insight into application of CT for development of FDM process at the design stage in order to achieve parts with optimal mechanical strength.

## 2 Materials and methods

### 2.1 Material, design, and fabrication process

An Ultimaker2 FDM printer was used for fabrication of the specimens. The material was black PLA filament with 2.85 ± 0.1 mm in diameter with melting temperature of 145–160 °C and glass transition temperature of 60–65°C [19]. The tensile specimens were manufactured according to the ISO 527 standard [20]. Figure 1a shows the CAD design and the fabrication orientation of the tensile specimens where the $Z$ direction is the build direction. The manufacturing parameters for fabrication of specimens including build direction, part orientation, printing speed, etc. were identical except the fabrication temperature. Different temperatures ranging from 180 to 260 °C with 10 °C increment were used resulting in nine sets of samples. For each fabrication temperature, three samples were fabricated for the tensile testing. The diameter of the extrusion nozzle was 0.8 mm for all the specimens. The layer thickness was 0.1 mm and 100 % infill was chosen for all the specimens. Build plate temperature and the nozzle travel speed were set to 60 °C and 70 mm/s respectively.

The infill pattern which was chosen for fabrication of the specimens is schematically illustrated in Fig. 1b, c. As it is shown in the figure, apart from the external contouring extruded filament, the specimens consisted of the longitudinal extruded filaments which were deposited along the $Y$-axis and transverse extruded filaments which were deposited along the $X$-axis of the specimens on the next layer. The fabricated specimens consisted of 20 layers of transverse and 20 layers of longitudinal extruded filament deposited on top of each other.

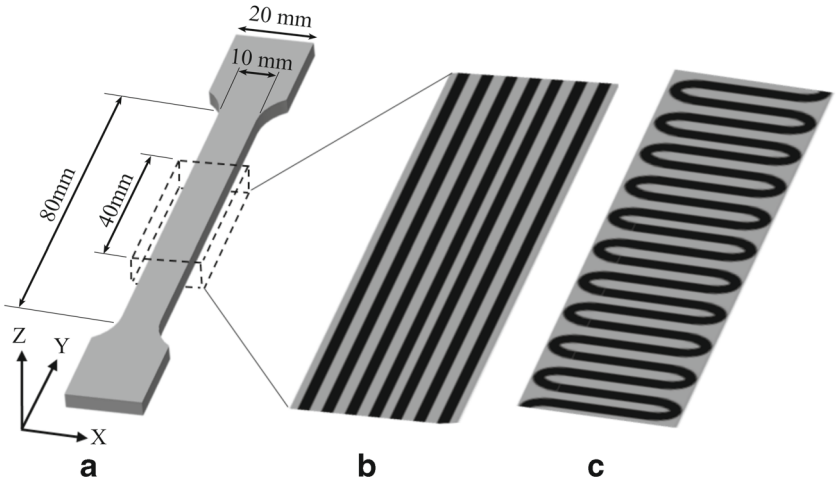


**Fig. 1** (a) CAD design and orientation of the specimens where the dashed box is showing the region of interest. (b) Schematic of longitudinal infill filaments. (c) Schematic of transverse infill filaments

## 2.2 Mechanical testing and measurement

The fabricated specimens were subjected to uniaxial tensile load until break in order to evaluate their tensile strengths. The tensile tests were performed at room temperature using an Instron 4458 instrument with a load cell of 300 kN. All tensile tests were performed at a speed of 1 mm/min.

## 2.3 X-ray computed tomography

In this study, a Nikon XT H 225 micro-computed tomography system was used. The CT parameters such as the number of projections, the tube power, and the magnification were set to be the same for all the scans. The CT scanning was done on one out of the three samples for each temperature. A 20-mm-long section of each specimen at the middle of the gauge length was scanned in order to achieve the desired resolution. The resulting voxel size for all the scans was 15.9 $\mu$m. The scanned section or the region of interest (ROI) is shown in Fig. 1a using the dashed box. One thousand eighty projections were captured in each scan while the voltage and amperage of the tube were 80 kV and 81 $\mu$A respectively. No filter was used in the scans and exposure time was set to 1 s.

The post-processing of CT data can affect the measurements and consequently the results. Adjusting the threshold in order to segment the material from the surrounding air which is called surface determination can be done based on different methods. In this study, ISO50 was used as surface determination method. This threshold-based segmentation method calculates the gray value of material and air peak from the data set histogram and considers the average value of those gray values as the threshold.

### 2.3.1 Minimum cross-sectional area

Since the specimens were subjected to a uniaxial tensile load, the measurement of minimum cross-sectional areas perpendicular to load direction was of interest. Such a measurement was operator dependent and highly dependent on the alignment of the reconstructed CT volumes; thus, a repeatable method must be used. In addition, due to the flaws affiliated with the fabrication process, the minimum load-bearing areas might not necessarily occur in a plane perpendicular to the load direction. Therefore, average of cross-sectional areas at several planes where the largest air gap volumes occur was measured instead. Aligned measuring boxes with specific thicknesses were used in VGStudio Max 3 in order to calculate the total volume of PLA material within the boxes. The average of the minimum cross-sectional area was calculated by dividing the volumes by the thickness of measuring boxes. This is further discussed in Section 3.2.2.

### 2.3.2 Porosity analysis

Using the CT data, the total volume of PLA material, as well as total volume of air trapped in each specimen at the ROI, was measured. The porosity of the specimens was calculated by dividing the air volume by sum of air plus material volume as it is shown in Eq. 1. The "material content" can be achieved by calculating the inverse of the porosity content.

$$Porosity = \frac{V_{air}}{(V_{air} - Vmaterial)} \tag{1}$$

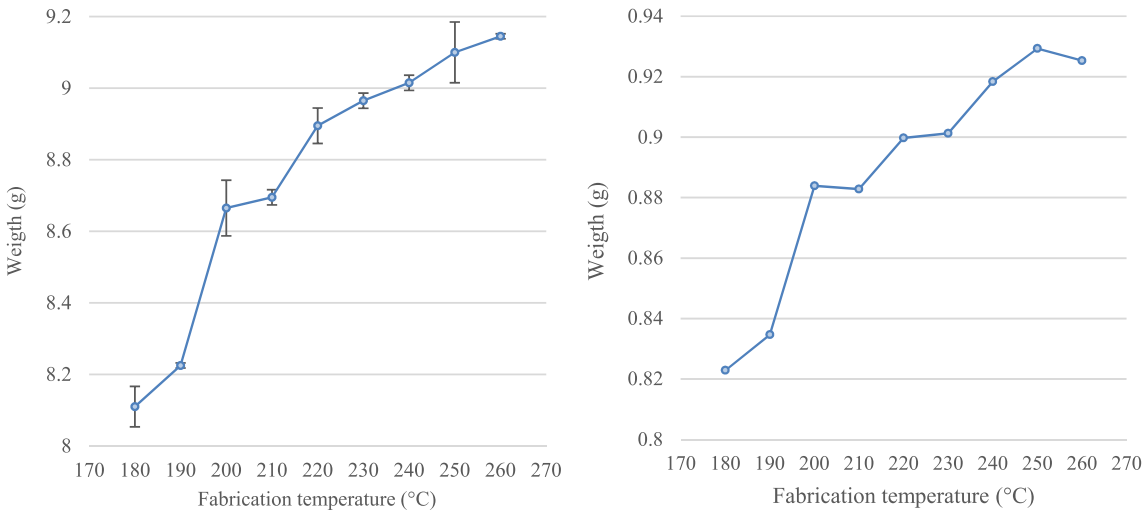


**Fig. 2** (Left) Average weight of specimens in gram. (Right) Weight of specimens at ROI calculated based on volumes obtained using CT

## 3 Results and discussion

### 3.1 Part quality

The weight of specimens was influenced by the selected fabrication temperatures. The specimens which were manufactured at higher temperatures were heavier regardless of their as-built geometry. Figure 2 shows the average weight of the specimens fabricated at different temperatures as well as the calculated weight of the specimens at ROI obtained from CT data based on their volumes. Both measurements obtained from total weight measurement of the whole specimens and weight measurement of ROIs from CT show the same trend. While the specimens printed at 180 °C and 190 °C have considerably lower total weight compared to the rest of the specimens, the deviation in weight for samples fabricated at 220 °C and higher was not significant. The same pattern can be observed from data acquired from weight measurement of ROI. The results from weight measurement show relative lack of deposition for specimens fabricated at lower temperatures.

The as-built geometry of specimens showed deviation from the CAD-designed geometry. Poor part quality compared to the rest of specimens was observed for the specimens fabricated at 180 °C and 190 °C. They had lower surface quality and the printer failed to deposit material at few regions due to inconsistent deposition rate. Figure 3a, b, c shows the CT-reconstructed geometry of specimens at ROIs fabricated at 180, 220, and 260 °C respectively. The aforementioned inaccuracy could be specifically observed at the side walls of the specimens fabricated at two lowest temperatures and it is shown for 180 °C in Fig. 3a. This can also be observed at a cross-section of the specimen fabricated at 180 °C in Fig. 4d.

The width of specimens was bigger than the designed width on the side facing to the build plate especially for those fabricated at 230 °C and higher. This was mainly due to the preheating of build plate. The cooling fans

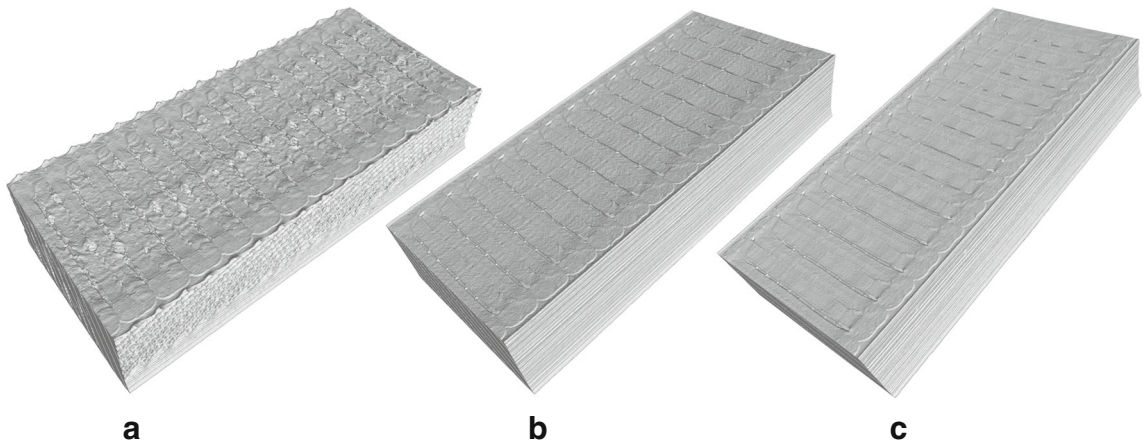


**Fig. 3** CT-reconstructed geometry of ROIs for specimens fabricated at **a** 180 °C, **b** 220 °C, and **c** 260 °C

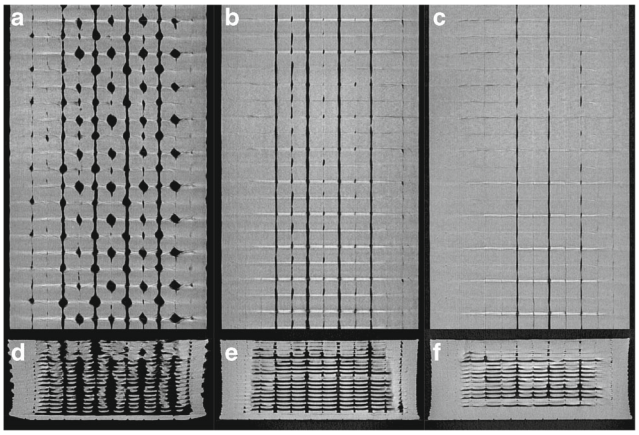


**Fig. 4** Cross-sectional areas of specimens fabricated at 180 °C, 220 °C, and 260 °C at **a**–c *XY* plane and **d**–**f** *XZ* plane

of the system were also not activated for the first four layers. This resulted in a concave shape for the cross-section of specimens fabricated at 220 °C and 260 °C which is illustrated in Fig. 4e, f respectively.

## 3.2 Investigation of internal geometry using CT

An in-depth investigation was carried out on the internal geometry of the specimens at the ROI obtained from CT data. The lack of deposition resulting in bigger air gap was observed for the specimens fabricated at lower temperatures which confirms the results obtained from the weight measurement. Figure 4 shows different cross-sections of the specimens fabricated at 180, 220, and 260 °C illustrating the quality of extruded filaments. Figure 4a, d shows lack of bond between longitudinal extruded filaments as well as poor deposition. The longitudinal filaments at the center are not bonded to each other; however, the contour filaments and their adjacent longitudinal filaments are slightly fused to each other. Figure 4b shows the quality of the bond between longitudinal filaments for the specimen fabricated at 220 °C. As it can be observed, the bond quality has significantly improved compared to the specimen fabricated at 180 °C even though considerably large longitudinal air gap, especially at the middle, still exists. Figure 4c which refers to the specimen fabricated at 260 °C shows smaller air gap compared to those fabricated at lower temperatures as well as the better bond between longitudinal extruded filaments. Figure 4d, e, f shows the cross-sections of specimens fabricated at 180 °C, 220 °C, and 260 °C at their minimum cross-sectional areas. As it is illustrated, the extruded filament widths for the specimen fabricated at 180 °C are considerably smaller compared to those fabricated at 220 °C and 260 °C which consequently resulted in significantly bigger air gaps for the specimen fabricated at 180 °C. Lack of bond between longitudinal extruded filaments for 180 °C can be observed resulting in the least minimum cross-sectional area among all the specimen groups. Although the filaments width has increased for specimen fabricated at 220 °C, still significant air gap can be observed. The specimen fabricated at 260 °C achieved the largest minimum cross-sectional area which is displayed in Fig. 4f, even though it is still porous at the center.

The lower part of the specimen fabricated at 260 °C consisting of the first eight layers was dense and no air gap could be observed. The same fully dense region can be observed for the specimen fabricated at 220 °C in Fig. 4e; however, it only consists of the first four layers. Moreover, considering Fig. 4d, e, f, the contour extruded filaments or basically the side walls are relatively dense at all fabricating temperatures since they consist of only longitudinal contour filaments deposited on top of each other.

### 3.2.1 Transverse filaments and turn effect

In the case of longitudinal load, the transverse extruded filaments have less contribution to the strength of FDM parts compared to longitudinal filaments; however, the bond between transverse filaments may impact the final longitudinal strength of the parts. The result from CT data showed that temperature has a considerable impact at turns during deposition of transverse filaments. Figure 5a–i displays the quality of the bond between transverse filaments for various fabrication temperatures where top images show the *XY* plane view and bottom images show *YZ* plane view. As it is illustrated in the *XY* plane view, the transverse filaments in specimens fabricated at 230 °C and above have larger bond area in contact with their adjacent filaments and the filaments at turns are almost joined together; however, for those fabricated at 220 °C and lower, the filaments are not joined together and have weaker bonds at turns. It is also visible from in the images from the *YZ* plane view that filament widths have increased by increasing the fabrication temperature. The thickness of the solid layer at the bottom of the specimens is also dependent on temperature and is almost one fourth of the total thickness of the specimens fabricated at 250 °C and 260 °C.

### 3.2.2 Minimum cross-sectional area measurement

The air gaps between transverse extruded filaments or the minimum cross-sectional areas perpendicular to tensile load direction were measured using VGStudio Max 3 at ROIs for specimens in each fabrication temperature. The volume of material based on voxel count in a box with specific unit length was measured for each specimen at three locations

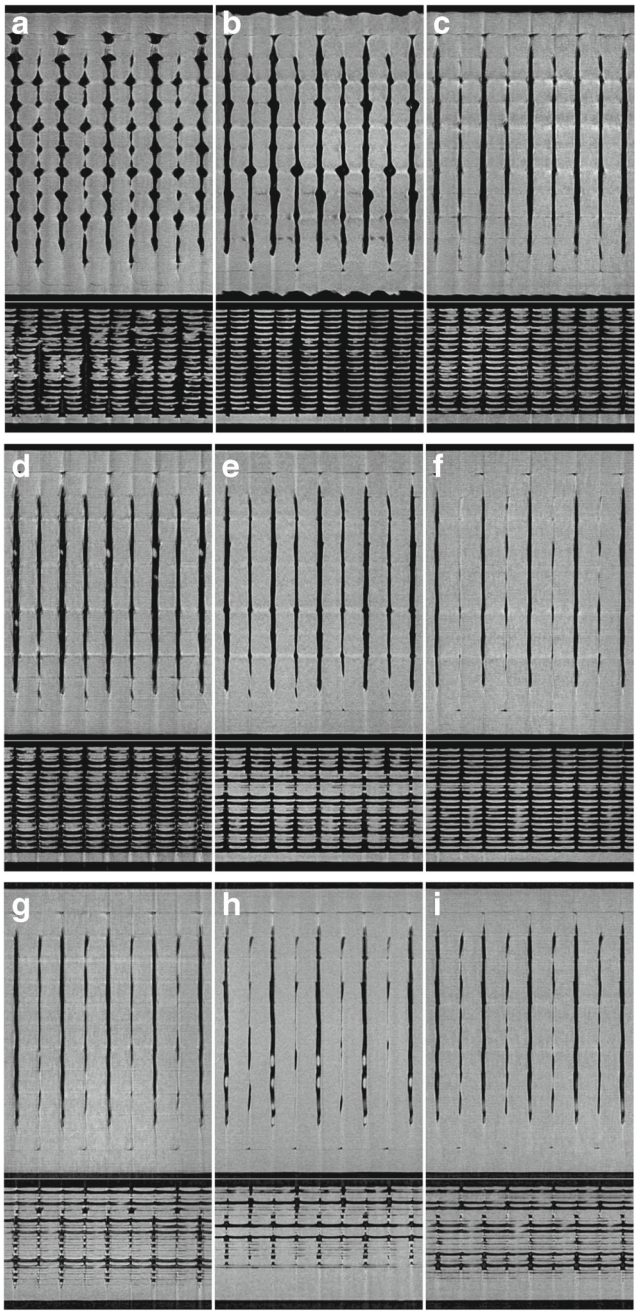


**Fig. 5** Bond quality of transverse filaments for specimens fabricated at **a** 180 °C to **i** 260 °C respectively (top *XY* plane and bottom *YZ* plane)

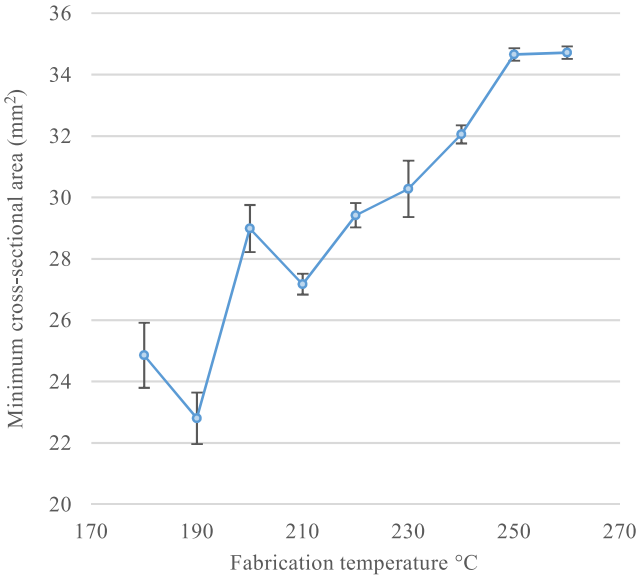


**Fig. 7** Average of minimum cross-sectional areas at ROI for the specimens fabricated at different temperatures

where minimum cross-sectional area occurred. By dividing the measured volumes by the thickness of the measuring boxes, the average of minimum cross-sectional area at the regions with the largest air gap volume was obtained for each specimen. Figure 6 illustrates the measuring boxes and their placement at the biggest air gap regions for the specimen fabricated at 190 °C. Figure 7 shows the average of minimum cross-sectional areas in square millimeters for various specimens calculated from CT data. As it can be seen in Fig. 7, the minimum cross-sectional areas are influenced by fabrication temperature. While the obtained values for the specimens fabricated at 180 and 190 °C were less than 25 $mm^2$, the specimens fabricated between 200 and 230 °C achieved minimum cross-sectional areas between 27.17 and 30.28 $mm^2$ respectively. The obtained values for the specimens with fabrication temperatures of 250 and 260 °C were nearly the same around 35 $mm^2$ which is 87.5 % of the nominal cross-sectional area.

### 3.2.3 Porosity analysis

The porosity values obtained from Eq. 1 using CT data showed a significant difference for the specimens. As it is illustrated in Fig. 8, the porosity values are influenced by fabrication temperature. As the fabrication temperature increases from 180 to 260 °C, the porosity content decreases by six times. The porosity content for the specimens fabricated at 180 °C and 190 °C is considerably higher in comparison to that of the rest of the specimens. Those fabricated between 200 and 230 °C had the porosity content between 5 and 7 % while those fabricated at 240 °C and higher had less than 3 % porosity. The porosity content did not change significantly in specimens fabricated at 240 °C and higher and it was nearly the same for the specimens fabricated at 250 and 260 °C. In the fabrication temperatures between 210 and 250 °C, the porosity changes linearly with temperature change and it can be obtained using the following empirical formula: $\text{Porosity}(\%) = -0.13 \cdot \text{fabrication temperature}\ (^{\circ}C) + 35$.

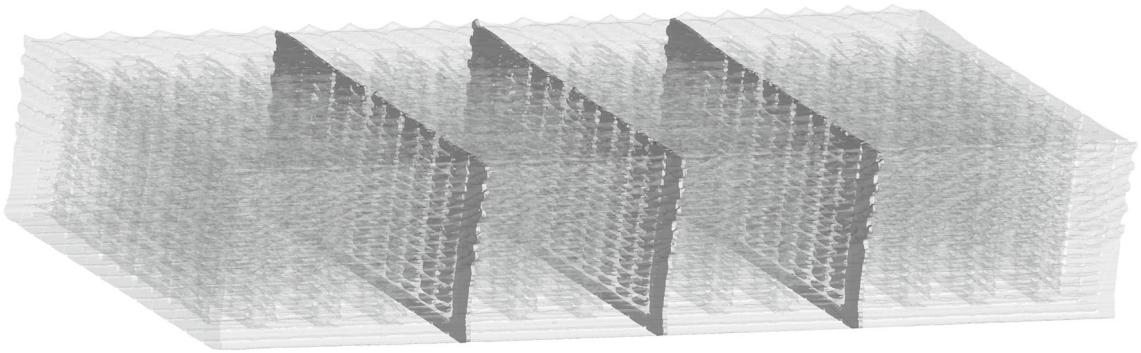

**Fig. 6** Porosity in ROI for the specimen fabricated at 190 °C and the three aligned measuring boxes

### 3.3 Mechanical strength evaluation

All the specimens were subjected to a uniaxial tensile load. The results showed that the mechanical properties of PLA specimens are dependent on fabrication temperature. The specimens fabricated at lower temperatures had a higher percentage of elongation and lower yield stress. On the contrary, those fabricated at higher temperatures showed higher yield stress and lower strain at break. In addition, different Young's modulus values were obtained for the specimens fabricated at different temperatures. Table 1 shows the average of tensile strength, Young's modulus, and strain at break for the specimens.

As it is presented in Table 1, the tensile strength has a linear relation to the fabrication temperature. Higher fabrication temperature resulted in higher uniaxial tensile strength. The specimen printed at 190 °C did not follow the linear pattern which can be referred to its lower measured minimum cross-sectional area. Different percentage elongation values were obtained depending on fabrication temperature. In general, increasing the fabrication temperature resulted in lower strain at break; however, specimens printed at 180 and 190 °C did not follow the linear transition which was observed for the specimens fabricated between 200 and 260 °C.

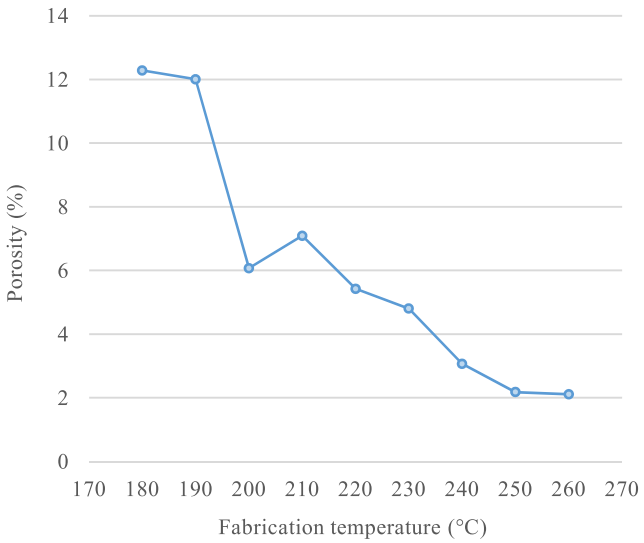


**Fig. 8** Porosity content for different fabrication temperatures

The tensile strength values were recalculated in order to account for the internal geometry of the specimens in relation to their strength. Therefore, the tensile strength values were divided by the corresponding material content value which resulted in the specific strength of each specimen based on its porosity. The material contents of each specimen were obtained from their corresponding porosity content. The result of such recalculation is presented in Fig. 9. Normalizing the strength values obtained from the tensile test by their material content for each fabrication temperature resulted in higher specific strength values. The resulted values which are an indication of the strength based on the porosity content have also a linear correlation to the fabrication temperature and follow the same trend as the strength values obtained directly from the tensile test. It should be considered that such a normalization had a bigger impact on the values obtained from lower temperature rather than those obtained from higher temperatures. The tensile strength value for the specimens fabricated at 180 and 190 °C had an average increase of 14 and 13.65 % respectively, while the increase for the specimen fabricated at 250 and 260 °C was only 2.23 and 2.15 % respectively.

The obtained strength values were also normalized based on the corresponding minimum cross-sectional area obtained from CT. The obtained minimum cross-sectional values from CT were divided by the nominal cross-sectional area of 40 $mm^2$ which was the input value of tensile testing resulting in the corrected area for each fabrication temperature. The tensile strength obtained from the tensile test was divided by corrected area values as are shown in Fig. 9. The resulted specific strength falls within a specific range for all the specimens which as it was expected was close to the tensile strength of bulk material which was

**Table 1** Uniaxial tensile test results

| Fabrication temperature °C | Tensile strength (MPa) | Young's modulus (GPa) | Strain at break (%) |
|---|---|---|---|
| 180 | 25.77 ± 0.5 | 2.25 ± 0.0 | 3.06 ± 0.0 |
| 190 | 24.29 ± 0.7 | 2.21 ± 0.1 | 3.07 ± 0.5 |
| 200 | 29.93 ± 1.7 | 2.75 ± 0.1 | 3.56 ± 0.4 |
| 210 | 31.74 ± 1.0 | 2.77 ± 0.1 | 3.23 ± 1.1 |
| 220 | 33.49 ± 0.7 | 2.95 ± 0.1 | 2.93 ± 0.3 |
| 230 | 34.15 ± 1.3 | 2.81 ± 0.1 | 2.89 ± 0.4 |
| 240 | 34.69 ± 0.4 | 2.86 ± 0.0 | 2.40 ± 0.4 |
| 250 | 37.38 ± 0.4 | 2.93 ± 0.1 | 2.33 ± 0.1 |
| 260 | 37.79 ± 2.0 | 3.05 ± 0.1 | 2.20 ± 0.1 |

pulled separately (45.59 MPa). The deviation in the obtained result can be referred to the fact that the minimum cross-sectional areas of fractured areas are not necessarily the same as the in-plane measured areas from CT.

Figure 10 displays the median force-displacement curve of specimens fabricated at 180, 220, and 260 °C. It can be observed that the specimen fabricated at 260 °C has higher tensile strength while it resulted in more brittle behavior compared to the specimens fabricated at 220 and 180 °C. The specimens fabricated at 180 °C showed more ductile behavior and relatively more elongation at break compared to those fabricated at 260 °C. Considering the obtained curves, it is also clear that for the same amount of force especially below 1 kN or basically in the elastic region, almost same displacement values for the specimens fabricated at 220 and 260 °C were obtained. It can be concluded that different failure mechanisms have taken place for different specimens which can be referred to the porosity content and the difference in the internal geometry of the specimens.

### 3.4 General remarks

Considering the CT investigations, the longitudinal extruded filaments in the specimens fabricated at temperatures higher than 230 °C had a larger bond area to their adjacent extruded filaments resulting in considerably smaller air gap compared to the specimens printed at 220 °C and below. The transverse filaments followed the same pattern with more severe lack of bond for the specimens printed at 220 °C and below. In addition, all the specimens even those fabricated at higher temperatures had inhomogeneous internal structure meaning that the porosity or local density for each specimen varied at different regions especially at side walls and bottom compared to center of the specimens.

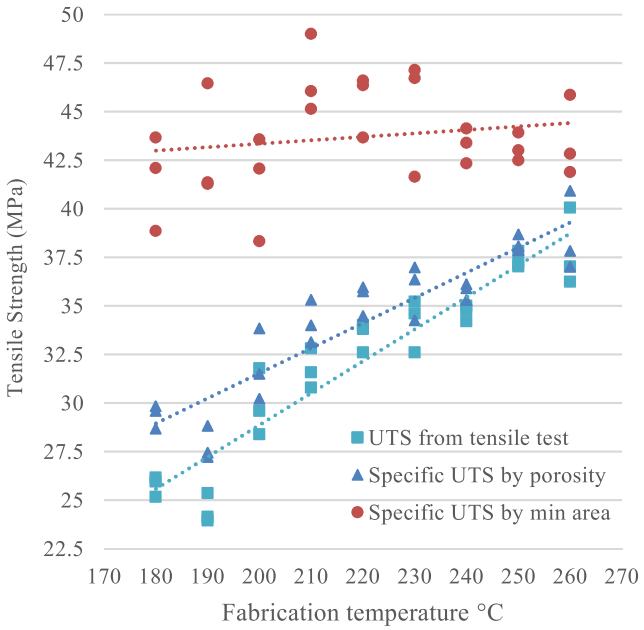


**Fig. 9** Specific strength values calculated based on CT results

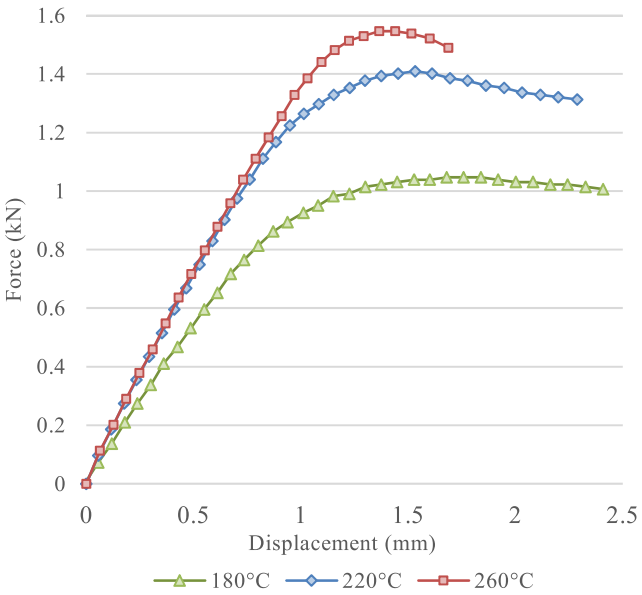


**Fig. 10** Force-displacement curves of specimens printed at 180, 220, and 260 °C

The bottom of all specimens, consisting the initial deposited layers, had the least porosity. This can be referred to the build plate preheat which contributes to better fusion for all extruded filaments regardless of their directions. The contour extruded filaments making the side walls which consisted of only longitudinal extruded filament deposited on top of each other and the bottom solid layer resulted in a highly dense U-shaped geometry at the gauge length of all specimens. This U-shaped geometry was relatively bigger for specimens fabricated at 220 °C and higher, especially for 250 °C and 260 °C. Apart from the thick solid bottom layer, the wall regions were also bigger since the turns from transverse filaments fusing to contour filaments were also contributing to them. It is assumed that this part of specimens had an influential contribution to their tensile strength.

Due to inconsistent deposition, the transverse filaments in the specimens fabricated at lower temperatures were fused together neither at turns nor at the center. Therefore, the transverse layers in those specimens are assumed to act mainly as a connecting layer between the surrounding longitudinal filaments and have less contribution to the uniaxial strength. The quality of fusion between turns with their adjacent turns as well as the turns with the contour filaments also was poor compared to those in the specimens fabricated at higher temperatures. The effect of bond quality at turns on the mechanical strength of FDM parts has been observed by Koch et al. [13]. The lack of fusion at turns caused that the longitudinal layers carry the load along the filaments while the transverse layers to act more like a spring. Figure 11 schematically shows the effect of fusion at turns on the elongation of different specimens. This phenomenon explains the higher percentage elongation and consequently lower Young's modulus for the specimens fabricated at the lower temperatures compared to those fabricated at higher temperatures which behaved more similar to a solid part achieving nearly the same percentage elongation at break of the bulk material. It was clear that width of extruded filaments at the center of the specimens was highly dependent on fabrication temperature. The width of extruded filaments deposited at higher temperatures was significantly bigger compared to those deposited at lower temperatures. Measurement of extruded filament width for various specimens was not repeatable since it was highly dependent on the cross-section at which the measurement was performed. Therefore, the porosity measurement and local minimum cross-sectional area were performed instead. Both the porosity and minimum cross-sectional area analyses confirmed lack of bond between extruded filaments at lower fabrication temperatures.

The porosity content is not necessarily the only influential factor on mechanical properties of PLA parts. The structure and orientation of porosity or air gaps with respect to the load play an important role. This means that the same amount of porosity content in the transverse direction can be much more critical than in the longitudinal direction in case of the longitudinal load. As it was shown, the air gaps in the transverse direction and their size showed to be the main factor for failure of investigated specimens. This basically made the quality of deposition in the transverse direction an important parameter in strength of parts. It can be concluded that by changing the fabrication temperature which eventually affects the quality of deposition in either transverse or longitudinal direction, it is possible to alter the mechanical properties of FDM parts in the desired direction.

Based on the CT results, the internal geometry of specimens was not homogenous due to inadequate deposition rate. Changing the nozzle travel speed selectively at various regions in accordance to fabrication temperature can be a solution for compensating the lack of deposition rate. This is especially more important during deposition at the turns where the tool path switches direction. By alternating FDM parameters with help of open-source slicing programs, it is possible to optimize the mechanical behavior of FDM for example parts with controlled anisotropic mechanical properties.

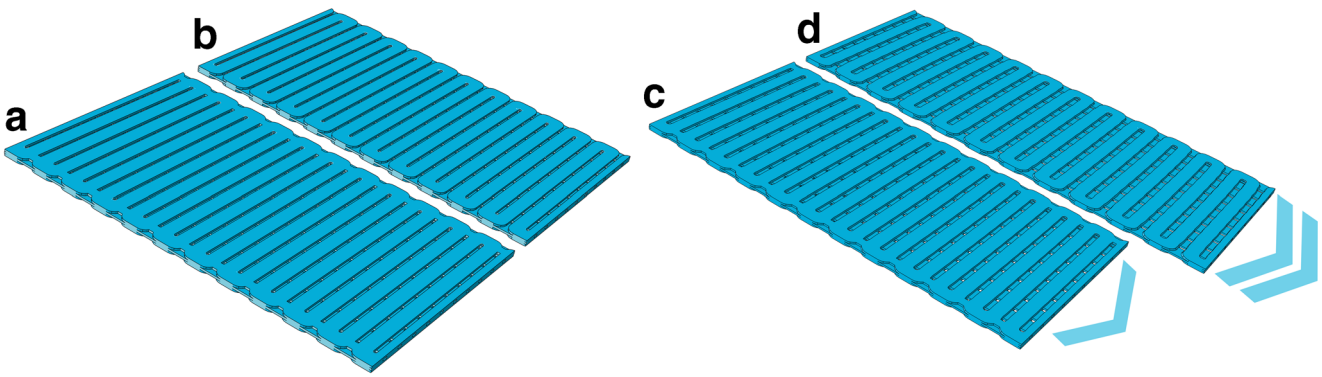


**Fig. 11** Schematic illustration of effect of turns in transverse layer. **a** Unloaded, specimen fabricated at high temperature. **b** Unloaded, specimen fabricated at low temperature. **c** Loaded, specimen fabricated at high temperature. **d** Loaded, specimen fabricated at low temperature

## 4 Conclusion

In this study, effects of temperature dependency on mechanical properties of PLA specimens fabricated using FDM have been investigated. CT as a non-destructive inspection tool has been used in order to study the effect of fabrication temperature on internal geometry of the specimens, especially on air gap measurement and the bond between deposited extruded filaments. Finally, uniaxial tensile testing was performed on all the specimens in order to evaluate the tensile strength of parts fabricated at different temperatures. The result has shown that for the parts fabricated at lower temperatures, the resulting air gaps between transverse extruded filaments are relatively big resulting in much smaller load-bearing cross-sectional area under uniaxial tensile load which consequently decreases the strength of the parts.

Using CT, it was shown that the local density varies throughout the parts regardless of fabrication temperature. This means that FDM parts, even those printed at recommended temperature range with 100 % infill, do not achieve homogenous internal structure. Since the porosity is not distributed homogenously throughout the FDM parts, it is not the only parameter for assessing the strength of FDM parts; however, internal geometry features such as minimum cross-sectional area obtained from CT give better information for evaluating the expected strength of FDM parts.

The results of this study show the importance of the application of CT as an inspection tool for development of FDM process. Using CT, it is possible to non-destructively study the internal structure of a part and use such information in order to achieve an optimum in-layer bond between filaments by minimizing the air gaps in the desired direction.



## References

1. Leering R (2017) 3D printing: a threat to global trade
2. Gebhardt A (2011) Understanding additive manufacturing, 1st edn. Carl Hanser Verlag GmbH & Co, KG. https://doi.org/10.3139/9783446431621
3. Gibson I, Rosen DW, Stucker B (2009) Additive manufacturing technologies: 3D printing, rapid prototyping, and direct digital manufacturing, 2nd edn. Springer Publishing Company, Incorporated, Berlin. https://doi.org/10.1007/978-1-4939-2113-3
4. Too M, Leong K, Chua C, Du Z, Yang S, Cheah C, Ho S (2002) Investigation of 3D non-random porous structures by fused deposition modelling. Int J Adv Manuf Technol 19(3):217. https://doi.org/10.1007/s001700200016
5. Zein I, Hutmacher DW, Tan KC, Teoh SH (2002) Fused deposition modeling of novel scaffold architectures for tissue engineering applications. Biomaterials 23(4):1169. https://doi.org/10.1016/S0142-9612(01)00232-0
6. Galantucci L, Bodi I, Kacani J, Lavecchia F (2015) Analysis of dimensional performance for a 3D open-source printer based on fused deposition modeling technique. Procedia CIRP 28:82. https://doi.org/10.1016/j.procir.2015.04.014
7. Pfeifer T, Koch C, Van Hulle L, Capote GAM, Rudolph N (2016) Optimization of the FDM additive manufacturing process. In: Proceedings of the annual technical conference (ANTEC) of the society of plastics engineers, Indianapolis, pp 22–29
8. Mohamed OA, Masood SH, Bhowmik JL (2015) Optimization of fused deposition modeling process parameters: a review of current research and future prospects. Adv Manuf:42–53
9. Kaveh M, Badrossamay M, Foroozmehr E, Hemasian Etefagh A (2015) Optimization of the printing parameters affecting dimensional accuracy and internal cavity for HIPS material used in fused deposition modeling processes. J Mater Process Technol 226:280. https://doi.org/10.1016/j.jmatprotec.2015.07.012
10. Villalpando L, Eiliat H, Urbanic RJ (2014) An optimization approach for components built by fused deposition modeling with parametric internal structures. Proced CIRP 17:800. https://doi.org/10.1016/j.procir.2014.02.050
11. Bellehumeur C, Li L (2004) Modeling of bond formation between polymer filaments in the fused deposition modeling process. J Manuf Process 6(2):170–178. https://doi.org/10.1016/S1526-6125(04)70071-7
12. Domingo-Espin M, Puigoriol-Forcada JM, Garcia-Granada AA, Llumà J, Borros S, Reyes G (2015) Mechanical property characterization and simulation of fused deposition modeling Polycarbonate parts. Mater Des 83:670. https://doi.org/10.1016/j.matdes.2015.06.074
13. Koch C, Van Hulle L, Rudolph N (2017) Investigation of mechanical anisotropy of the fused filament fabrication process via customized tool path generation. Addit Manuf 16:138. https://doi.org/10.1016/j.addma.2017.06.003
14. Chin Ang K, Fai Leong K, Kai Chua C, Chandrasekaran M (2006) Investigation of the mechanical properties and porosity relationships in fused deposition modelling-fabricated porous structures. Rapid Prototyp J 12(2):100. https://doi.org/10.1108/13552540610652447
15. Seppala JE, Migler KD (2016) Infrared thermography of welding zones produced by polymer extrusion additive manufacturing. Addit Manuf 12:71. https://doi.org/10.1016/j.addma.2016.06.007
16. Agarwala MK, Jamalabad VR, Langrana NA, Safari A, Whalen PJ, Danforth SC (1996) Structural quality of parts processed by fused deposition. Rapid Prototyp J 2(4):4. https://doi.org/10.1108/13552549610732034
17. Thompson A, Maskery I, Leach RK (2016) X-ray computed tomography for additive manufacturing: a review. Measur Sci Technol 27(7):072001. https://doi.org/10.1088/0957-0233/27/7/072001
18. Nouri H, Guessasma S, Belhabib S (2016) Structural imperfections in additive manufacturing perceived from the X-ray micro-tomography perspective. J Mater Process Technol 234:113. https://doi.org/10.1016/j.jmatprotec.2016.03.019
19. Ultimaker, Technical data sheet PLA Version 3.003. Technical report (2016)
20. International Organization for Standardization. ISO 527-2:2012 Plastics – Determination of tensile properties – Part 2: Test conditions for moulding and extrusion plastics (2012)